Self-scaling Kinematic Hand Skeleton for Real-time 3D Hand-finger Pose Estimation

Kristian Ehlers and Jan Helge Klüssendorff
Institute of Computer Engineering, Universität zu Lübeck, Lübeck, Germany

Keywords: Hand-finger Pose Estimation, Self-scaling Kinematic Skeleton, Hand Skeleton Tracking, Gesture Detection

Abstract: Since low cost RGB-D sensors have become available, gesture detection has gained more and more interest in the field of human computer and human robot interaction. It is possible to navigate through interactive menus by waving one's hand and to confirm menu items by pointing at them. Such applications require real-time body or hand-finger pose estimation algorithms. This paper presents a kinematic approach to estimate the full pose of the hand including the angles of the finger joints. A self-scaling kinematic hand skeleton model is presented and fitted into the 3D data of the hand in real-time on standard hardware with up to 30 frames per second without using a GPU. This approach is based on the least-square minimization and an intelligent choice of the error function. The tracking accuracy is evaluated on the basis of a recorded dataset as well as simulated data. Qualitative results are presented to emphasize the tracking ability under hard conditions like full hand turning and self-occlusion.

1 INTRODUCTION

Gestures are part of our daily lives, e.g., some people gesticulate while they are talking to emphasize their intention and young children point at things they would like to have. People greet each other over larger distances by simply waving their hand and policemen control the traffic with certain arm movements.

As gestures are a common, intuitive, and simple form of communication, human pose estimation and gesture detection are gaining more and more interest in the field of human computer interaction (Han et al., 2013). They can be used for the touchless control of applications or to play games on consoles like the Xbox 360 in combination with the low-cost RGB-D sensor Microsoft Kinect, which can generate a 3D point cloud of the scene in front of the camera. In such use cases, gestures are defined on the basis of movements or the arrangement of body parts like swiping the hand or jumping.

Regarding applications with limited space in front of the camera, full body movements are unfavorable. Therefore, specific poses of the hand and, in more detail, the fingers are defined as hand or hand-finger gestures. For instance, the thumbs-up gesture is used to indicate that everything is fine and even sign language is based on hand and hand-finger gestures.

The detection of both body gestures and hand-finger gestures requires efficient algorithms to estimate and classify full body poses or hand-finger poses in real-time.

One of the major issues in estimating the pose of a human skeleton is the large state space. For example, the hand is a highly articulated object and it is often modeled using at least 26 degrees of freedom (Erol et al., 2007; ElKoura and Singh, 2003; Oikonomidis et al., 2010).

However, this paper proposes an approach for full hand-finger pose estimation based on a self-scaling kinematic hand skeleton model: the positions of the fingers' joints and other features like the fingertips as well as the joints' angles are estimated by using inverse kinematics and simple model data distances to solve the formulated optimization problem. Further, the model determines the wrist's joint position describing the relation between hand and arm. Since the size of the human hand varies and a standard kinematic skeleton has a fixed size, the presented kinematic skeleton is scaled during the optimization process. This approach uses the data of one single depth camera and is not limited to human hands but can be extended to arbitrary skeletons.

A support vector machine (SVM) is trained with different hand-finger poses and used for the finger gesture classification.

The pose estimation approach is evaluated in detail with respect to fingertip tracking accuracy and performance as well as the correct determination of the hand's configuration, i.e., the joints' angles. Determining the wrist's joint position requires the 3D

Ehlers K. and Klüssendorff J..
Self-scaling Kinematic Hand Skeleton for Real-time 3D Hand-finger Pose Estimation.
DOI: 10.5220/0005257501850196
In *Proceedings of the 10th International Conference on Computer Vision Theory and Applications* (VISAPP-2015), pages 185-196
ISBN: 978-989-758-090-1

points of a small part of the arm. As is known to the authors, the available datasets do not contain this information, which is why no usable datasets of annotated hand skeletons and depth images are available (Oikonomidis et al., 2010; Schröder et al., 2013; Sridhar et al., 2013; Qian et al., 2014). Therefore, ground truth data is generated while robot-based movements of a gypsum hand model are recorded and some hand movements performed by a test subject are recorded and annotated. In addition, the self-scaling ability is evaluated and joint movements are simulated to determine the correctness of the joint position estimation. Moreover, the results of qualitative evaluation and performance tests are presented.

Hence, the hand pose estimation is based on the 3D data of the hand an approach for the initial detection of the hand points is presented.

This paper is organized as follows: Section 2 describes related work on hand-finger pose estimation and finger gesture detection and presents some of the main differences to the developed method. An approach to detect the hand inside a 3D scene, the kinematic hand skeleton model including the finger pose estimation approach, and a gesture classifier based on the joints' angles are presented in Section 3. Experiments and detailed evaluations are given in Section 4 followed by the conclusion presented in Section 5.

2 RELATED WORK

There are several approaches to estimate the pose of the human hand using RGB or RGB-D image data. Some of them are based on large datasets, calculated beforehand, or a specific hand model. Sometimes markers have to be worn whereas other approaches are completely markerless.

Ren et al. determine the hand pose in the form of finger gestures by introducing the Fingers-Earth Mover's Distance as a distance metric for hand dissimilarities (Ren and Yuan, 2011; Ren et al., 2011). The fingers are matched on the basis of the hand shape given by the depth image of the Kinect. The current gesture is determined by template matching on a dataset, recorded beforehand.

Athitsos et al. determine plausible 3D hand configurations by formulating image database indexing problems (Athitsos and Sclaroff, 2003). For this purpose, they compute a large database consisting of synthetic hand images by rendering 26 basic shapes of an articulated hand model at different orientations. Given the current hand image, the algorithm matches the corresponding edge image with the database edge images by determining image distances like the chamfer distance. The closest match directly represents the current hand configuration.

Horaud et al. estimate a hand model based on 3D data by matching an articulated hand shape model using robust point registrations with expectation conditional maximization (Horaud et al., 2011).

De La Gorce et al. recover the 3D hand pose from monocular images through the minimization of an objective function using a quasi Newton approach based on a parametric hand model (Gorce et al., 2011). The objective function includes texture and shading information to handle self-occlusions and the well-defined image formation process determines a synthetic hand image as similar as possible to the current image based on the articulated hand model and the RGB image.

Oikonomidis et al. determine the hand skeleton based on a particular model and Particle Swarm Optimization (PSO) (Oikonomidis et al., 2010; Oikonomidis et al., 2011). The pose of the hand is determined by the minimization of an error function using PSO, whereby it is based on skin and edge feature maps of the current hand image and hypothesized poses.

Besides the aforementioned methods, there are approaches that use markers to estimate the pose of the hands. Thus, the approach of Wang and Popović is based on a glove, colored with a specific pattern, and a recorded dataset containing rasterized glove images of natural hand poses (Wang and Popović, 2009). Therefore, the current hand pose is estimated by finding the best matching image in the database with respect to a robust distance metric. Schröder et al. extend this approach to control an anamorphic robot hand (Schröder et al., 2012). They save the pose-specific parameters of a kinematic hand model and use them to render the corresponding glove images needed for the pose estimation.

In (Keskin et al., 2011), the authors present a randomized decision forest (RDF) approach for hand pose estimation. They adapt the well-known body pose estimation approach of (Shotton et al., 2011) and train a decision forest with hand pose data. They extend their approach to a multi-layered RDF network in (Keskin et al., 2012) by developing a hand shape RDF. For each hand shape, a special RDF is trained to determine the parts of the hand.

The aforementioned approaches are based on large datasets recorded beforehand or calculated data such as decision forests. They often need to be processed by the GPU to achieve acceptable frame rates. This paper presents a real-time approach running with up to 30 frames per second (FPS) on standard hardware without GPU acceleration.

Aristidou and Lasenby propose an algorithm to iteratively adapt the joints of a kinematic hand model using inverse kinematics and a marker-based optical motion capturing system (Aristidou and Lasenby, 2010).

In (Schröder et al., 2013), the authors use inverse kinematics to fit a virtual hand model into the 3D data of the hand. The model consists of a triangulated mesh with a kinematic hand skeleton. A least-squares optimization is used to adapt the model to the 3D point cloud. Therefore, the distance between the model and the current data is determined by the point-to-triangle distance.

In (Liang et al., 2012), the authors present a three-step Iterative Closest Point (ICP) based approach for hand pose estimation based on an articulated 3D mesh model. The global motion estimation is performed by overlaying the current hand data with the model data using the ICP method on the current hand data and the corresponding model's visible mesh points. Further, a fingertip estimation and inverse kinematics result in a first aligned model. The final step is the articulated ICP to align the mesh model and the real data.

Ballan et al. also fit meshed hand models with underlying skeletons into 3D data and extend the application to interactions of both hands with objects, e.g., holding a small ball or folding the hands. They use multiple camera views to handle mutual occlusions (Ballan et al., 2012). There are other approaches covering human-object interaction tasks like grasping, hand manipulation tasks, or hand tracking for computer aided design (Wang et al., 2011; Wang et al., 2013; Zhao et al., 2013).

Nevertheless, this paper concentrates on the task of hand-finger pose estimation and introduces a kinematic model-based approach differing from the named ones in all ways except the usage of a kinematic model but with the addition that it is self-designed and extended. The kinematic skeleton is directly fitted into the visible hand data corresponding to the hand's surface. The offset between the hand surface and the bones is ignored during the non-linear least square optimization process and leads to a simpler data-model distance as presented in (Schröder et al., 2013). This simplification speeds up the whole pose estimation. Further, it allows to handle motion-depending self-occlusions and just one optimization process is needed. In addition, the kinematic model is extended by an arm stub representing the pose information between hand and arm. One of the main improvements with respect to other kinematic model approaches like (Qian et al., 2014) is the model's self-scaling ability. The skeleton is scaled during the whole estimation process and can handle every hand size automatically.

To the authors' knowledge, the approach of Qiang et. al presented in (Qian et al., 2014) is the only one that achieves a robust hand-finger pose estimation with a speed up to 25 FPS. Qiang et. al use a kinematic hand motion model with 26 degrees of freedom and combine the ICP and PSO optimization to realize full articulated hand tracking based on the data of Intel's Creative Interactive Gesture Camera. They use a sphere-based hand model and sample the hand's point cloud down to 256 points to achieve real-time performance.

Despite the resulting high number of 29 degrees of freedom of the kinematic skeleton presented here, the pose estimation runs in real-time with 30 FPS, limited by the camera without any use of the GPU. In addition, the data of the hand is not sampled down. The real-time performance of 30 FPS is achieved using the nearly 16.000 points of the hand in a distance of 50 cm to the camera as well as by using the 5.500 points in a distance of 100 cm. The efficiency and the fact that there is no need for previously calculated large datasets allow for real-time performance and would predestinate this approach for embedded applications.

For some approaches, multiple steps are necessary to estimate the hand-finger pose, e.g., determination of the hand shape or the finger tips followed by the determination of the full hand pose (Liang et al., 2012; Keskin et al., 2012). The presented approach needs only one optimization process based on the simple model data distance. Furthermore, the approach is not limited to the application of the hand pose estimation and it can deal with arbitrary kinematic skeleton models.

3 FINGER POSE ESTIMATION

The task of hand-finger pose estimation can be subdivided into two major problems: finding the hand inside the 3D scene and determining the pose. This section presents solutions for both problems. In the following, the full hand pose and the hand-finger poses, including the joints' angles of the fingers, are used synonymously.

3.1 Initial Hand Detection

One of the most challenging tasks, apart from estimating the full hand pose, is the initial localization of the hand inside a given 3D scene. Often many restrictions are made to the scene and hands' positions, e.g., cropping the whole scene or assuming the hand is the closest object to the camera (Ren et al., 2011).

This paper presents a simple and more flexible approach assuming a static camera and only one human being inside the scene facing the camera. The first depth image is stored as reference. For each frame, the difference image with respect to the reference image is calculated. Afterwards, a blob detection is performed and the largest blob is assumed to represent the human being. In each step, the reference image is adapted to the current scene by updating a depth value if the current value is larger than the corresponding one inside the reference image. After a while, the reference image represents the background. For a usable pose estimation, the hands should be situated in front of the human being. Thus, all points outside the blob as well as all points with a larger depth value than the mean depth value of the blob representing the human body reduced by a threshold of about 20 cm are removed. It is assumed that the two largest remaining blobs represent the hands. It is hard to distinguish the hands on the basis of their positions only, e.g., the arms can cross each other and a left hand facing the camera with the back of the hand looks like a right hand facing the camera with the palm. Hence, for initialization, it is assumed, that the palms of the hands face the camera.

The blob of a hand is examined in a similar way as presented in (Raheja et al., 2011). The estimation of the center of the palm is based on the distance transform and the palm-corresponding pixels are removed. The left sub blobs seem to be the fingers and allow to determine their tips. Since it is assumed that the open hand is presented for the initial hand detection, there have to be five finger blobs. The hand's orientation can be calculated by the mean value of the vectors defined by the palm's center and the fingertips. This information is used to initialize the kinematic skeleton's position and the orientation according to the z-axis of the camera.

3.2 Kinematic Hand Skeleton

In this paper, hand-finger pose estimation is not reduced to the determination of the positions of specific hand features like the fingertips or the center of the palm. It rather tends to estimate the joints' angles using a self-scaling kinematic model approach which also determines the joints' positions.

The kinematic hand model is designed in accordance with the human hand skeleton illustrated in Figure 1. It consists of nodes and edges corresponding to the skeleton's joints and bones. The carpal bones and the wrist joint are modeled by one central node (CEN) forming the anchor of the whole model. The basic coordinate system ($\mathrm{CS}_{\mathrm{CEN}}$) of the model is situated in the CEN where the z-axis faces the back of the hand, the y-axis faces the thumb, and the x-axis completes the right handed coordinate system facing the middle finger. All fingers and the so called arm stub are connected to the CEN. The arm stub represents the data inside the hand's 3D data corresponding to the lower arm's distal part. It consists of two nodes connected to each other and to the CEN via edges. The wrist can perform movements in two directions, i.e., flexion and extension as well as abduction and adduction. Therefore, the arm stub can be rotated around the z- and the y-axis of the basic coordinate system.

Each finger is modeled by four edges corresponding to the bones: the distal, medial, proximal phalangeal bones, and the metacarpal bone. The edges connect the nodes representing the distal (DIP) and proximal interphalangeal joints (PIP), the metacarpophalangeal joint (MCP), and the fingertip (TIP). The edge representing the metacarpal bone is directly connected to the central node. Each finger is allowed to perform extension and flexion in all three joints as well as abduction and adduction in the MCP.

To keep the model simple, the thumb is treated as a normal finger, although it has got no medial phalangeal bone. Hence, it is modeled in a way that the model's distal phalangeal edge corresponds to the thumb's phalangeal bone, the model's medial phalangeal edge corresponds to the thumb's proximal phalangeal bone, and the model's proximal phalangeal edge corresponds to the thumb's metacarpal bone. The model's metacarpal edge bridges the distance between the thumb's carpometacarpal joint and the CEN. Consequently, in contrast to the fingers' carpometacarpal joints, the thumb's carpometacarpal joint is modeled to be flexible in two directions.

The kinematic hand model is described with the aid of the Denavit-Hartenberg (DH) transformations. If the joints' coordinate systems are situated in accordance with the DH conventions, the transformation from a coordinate system CS_i to another one CS_{i+1} can be described with the following four parameters: d - offset between both coordinate systems' origins along the z_i-axis, θ - rotation angle around the z_i-axis to overlay x_i and x_{i+1}, a - offset between both coordinate systems' origins along the x_{i+1}-axis, and α - rotation angle around the x_{i+1}-axis to overlay x_i and x_{i+1}. The rotation inside a joint is given by the angle θ around the z-axis of the joint's coordinate system.

Each finger is modeled by a kinematic chain consisting of five coordinate systems, one for each joint's movement axis and one for the fingertip. Figure 1(b) illustrates the way the model is placed inside the hand based on the back view of the right hand. The first coordinate system ($\mathrm{CS}_{\mathrm{MCP1}}$) is situated at the MCP node

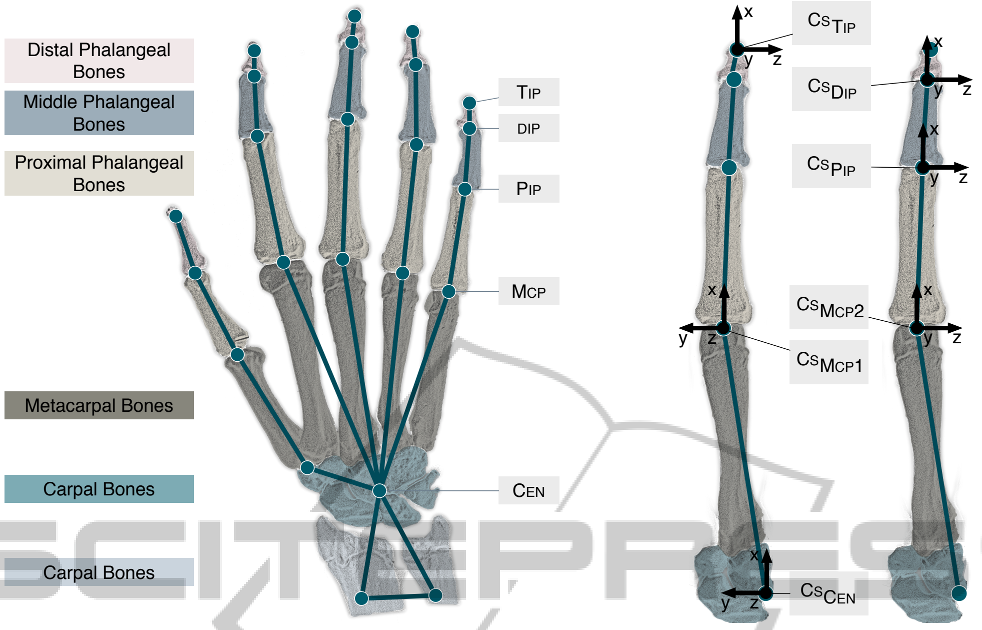

(a) (b)

Figure 1: Back view of the kinematic hand skeleton model of the right hand. (a) The nodes are situated at the joint's positions and connected via edges to rebuild the human hand skeleton. All fingers and the thumb are modeled in the same way. Since the thumb has no middle phalangeal bone, the model's joint corresponding to the metacarpophalangeal joint is situated inside the carpometacarpal joint. (b) Each finger is modeled as a kinematic chain of the finger joints and the fingertip at the end. All five chains are connected to the central node situated at the central point of the wrist bones. The hand's pose is given as the pose of its basic coordinate system CS$_{\text{CEN}}$ situated in the basic hand node CEN.

Table 1: Kinematic model's DH parameter from CS$_{\text{MCP1}}$ to CS$_{\text{TIP}}$. The rotation inside a joint is given by the corresponding θ. The length of the edges representing the phalangeal bones are given by a.

Finger joint	DH-Parameter			
	l	θ	a	α
CS$_{\text{MCP1}}$ - CS$_{\text{MCP2}}$	0	θ_{MCP1}	0	$\pi/2$
CS$_{\text{MCP2}}$ - CS$_{\text{PIP}}$	0	θ_{MCP2}	$a_{\text{MCP}-\text{PIP}}$	0
CS$_{\text{PIP}}$ - CS$_{\text{DIP}}$	0	θ_{PIP}	$a_{\text{PIP}-\text{DIP}}$	0
CS$_{\text{DIP}}$ - CS$_{\text{TIP}}$	0	θ_{DIP}	$a_{\text{DIP}-\text{TIP}}$	0

realizing the abduction and adduction. The origin of the second coordinate system (CS$_{\text{MCP2}}$) overlays CS$_{\text{MCP1}}$'s origin and realizes the flexion and extension inside the metacarpophalangeal joint. The same movements inside the interphalangeal joints PIP and DIP are modeled by CS$_{\text{PIP}}$ and CS$_{\text{DIP}}$. To determine the fingertip's position, the coordinate system CS$_{\text{TIP}}$ is situated in TIP. Thus, the kinematic chain of a finger is given by CS$_{\text{MCP1}}$ - CS$_{\text{MCP2}}$ - CS$_{\text{PIP}}$ - CS$_{\text{DIP}}$ - CS$_{\text{TIP}}$ and the corresponding DH parameters listed in Table 1.

As CS$_{\text{CEN}}$ is the anchor of the whole model, the pose of CS$_{\text{MCP1}}$ is determined by the translations along the x-, y-, and z-axes without any rotations except the thumb. The thumb's CS$_{\text{MCP1}}$ is rotated about 45° around the basic coordinate system's x-axis. The translation values and the lengths of the edges representing the interphalangeal bones define the size of the model and are determined by using a manual measurement of an X-Ray image of a hand.

The model has 28 degrees of freedom (DOFs), i.e., 20 rotations inside the finger joints, two rotations of the arm stub with respect to the CEN and the pose of the CS$_{\text{CEN}}$ inside the camera coordinate system described by three translations as well as the yaw, pitch, and roll angles inside the camera's coordinate system. The forward kinematic allows to estimate the hand's features' positions inside the camera coordinate system based on given joint and pose parameters corresponding to the described DOFs as well as the bone lengths. For instance, the position of a fingertip is given by

$$\text{TIP} = \text{T}_{\text{CS}_{\text{CEN}}} \cdot \text{T}_{\text{CS}_{\text{MCP1}}} \cdot \text{DH}_{\text{CS}_{\text{MCP2}}} \cdot \text{DH}_{\text{CS}_{\text{PIP}}} \cdot \text{DH}_{\text{CS}_{\text{DIP}}} \cdot \text{DH}_{\text{CS}_{\text{TIP}}} \cdot (0,0,0,1)^T \qquad (1)$$

with the pose matrices T$_{\text{CS}_{\text{CEN}}}$ - CS$_{\text{CEN}}$'s pose inside the camera coordinate system and T$_{\text{CS}_{\text{MCP1}}}$ - CS$_{\text{MCP1}}$'s pose inside CS$_{\text{CEN}}$. Furthermore, DH$_{\text{CS}_{\text{MCP2}}}$ to DH$_{\text{CS}_{\text{TIP}}}$

describe the poses of the corresponding coordinate system with respect to the previous coordinate system of the finger's kinematic chain and is described by the DH parameters (see Table 1) and the bone lengths. The poses of the other features can be determined by removing the unnecessary pose matrices from Equation 1, e.g., the position of $\mathrm{CS}_{\mathrm{MCP2}}$ is given by

$$\mathrm{MCP2} = \mathrm{T}_{\mathrm{CS}_{\mathrm{CEN}}} \cdot \mathrm{T}_{\mathrm{CS}_{\mathrm{MCP1}}} \cdot \mathrm{DH}_{\mathrm{CS}_{\mathrm{MCP2}}}(0,0,0,1)^T. \quad (2)$$

Since the bone lengths have to be defined in advance, the kinematic skeleton has a fixed size. To overcome this problem, the measured bone lengths as well as the values describing the position of the $\mathrm{CS}_{\mathrm{MCP1}}$ with respect to $\mathrm{CS}_{\mathrm{CEN}}$ are equipped with a global scaling factor α. This factor represents the 29th degree of freedom and is one of the main differences to kinematic models known from other approaches as presented in (Sridhar et al., 2013; Schröder et al., 2013; Ballan et al., 2012). Other differences are the additional arm stub nodes which are used to model the correspondence between hand and arm as the angles of the wrist joint. Further, the MCP joint of the thumb is simplified and initially rotated.

As suggested by other approaches, the joint angles are limited to prevent impossible hand-finger poses (Lee and Kunii, 1995).

3.3 Pose Estimation

Estimating the hand-finger pose means determining the 29 model parameters in a such way that the kinematic model represents the hand's 3D data, e.g, the fingertips should be situated at the center of all 3D points corresponding to the real fingertip. The same should be realized for all nodes of the model.

Assuming that the target positions of the model's nodes inside the current data are known, the model can be moved inside the center of the data and the parameters can be estimated using inverse kinematics with a non-linear least squares optimization approach and defining $f(\overline{p})$ as the positions of the model's nodes described in Section 3.2 depending on the 29 model parameters $\overline{p}$. Thus, $f(\overline{p})$ represents a vector containing the x-, y-, and z-coordinates of each node of the model. The optimization of the parameter vector $\overline{p}$ is done iteratively using a version of the Levenberg-Marquardt approach whereby the parameter vector $\overline{p}_{i+1}$ in the next iteration step is given by

$$\overline{p}_{i+1} = \overline{p}_i - (H + \mathrm{diag}[H])^{-1} \cdot J(\overline{p}_i)^T \cdot e(\overline{p}_i). \quad (3)$$

In this equation, $\overline{p}_i$ represents the model parameters at iteration step i, J and H are the Jacobian and Hessian matrices of f, and $e(\overline{p}_i)$ the error function depending on $\overline{p}_i$.

The choice of the error function is essential for the optimization of the parameter vector. Here, $\overline{t}_i$ is defined as the vector containing the node's target positions for the optimization corresponding to $f(\overline{p}_i)$ at iteration i and the error function $e(\overline{p}_i)$ is given as the difference vector

$$e(\overline{p}_i) = \overline{t}_i - f(\overline{p}_i). \quad (4)$$

Given the tracked kinematic skeleton of the previous frame and the current hand data as shown in Figure 2(a), the target position of a node is determined by the mean of all its assigned 3D points of the hand: all points with a smaller distance to this node than to all the other nodes of the model. The point assignment is illustrated in Figure 2(b). The skeleton determined on the basis of the previous frame is adapted to the target node positions illustrated in Figure 2(c). Determining the target point as described above, corresponds to fit the model into the hand's surface and is one of the simplifications made to accelerate the whole optimization process. In some applications or approaches, this distance between the surface and the real skeleton position is handled (Shotton et al., 2011; Schröder et al., 2013). Nevertheless, the coordinate systems of all joints are known and it is easy to determine the joint positions inside the hand by adding a simple offset along the joint's z-axis. The optimization of the parameter vector is performed for a predefined number of iterations and the assignment is renewed several times per point cloud, e.g., 20 iterations and renewals every four iterations are sufficient. Since the initial hand pose is unknown, it is expected that the initial pose is the open hand, i.e., all fingers should be extended. Furthermore, the hand detection approach described in Section 3.1 delivers the hand's orientation as the rotation angle around the camera's z-axis and the initial model parameters are set to zero except the hand's basic coordinate system's yaw angle and its position which is determined by the mean of the hand's 3D point cloud. In the following, the initial parameter vector used for the current point cloud is given by the resulting parameter vector of the previous image. The point cloud itself is determined by all points within a sphere with a predefined diameter around the model's current position.

The scaling is performed by including the global scaling factor α in the parameter vector. A major problem with the hand movements are self-occlusions, e.g., during a vertical rotation of the hand in front of the camera, the thumb and the index finger can cover the remaining fingers so that there is no 3D information corresponding to the fingers available. In such cases, no points are assigned to the corresponding model nodes and these nodes are ignored during the optimization process. This simple assumption al-

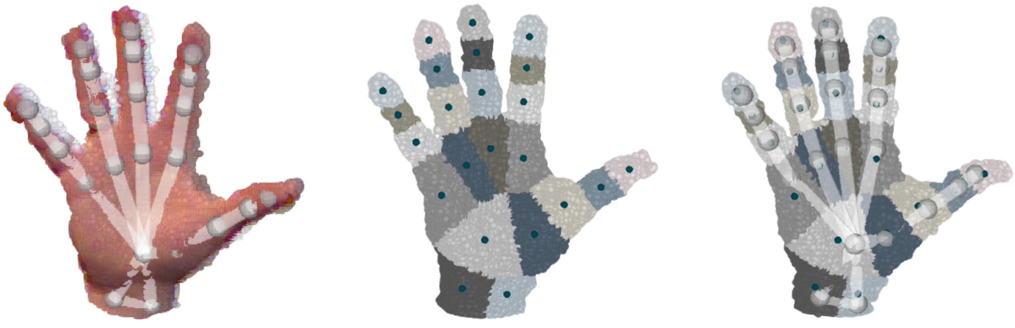

Figure 2: Determination of the target node positions. (a) Kinematic skeleton of the previous frame inside the current hand data. (b) The points assigned to the nodes and the target positions given by the corresponding mean values are highlighted as dark dots. (c) Adapted skeleton inside the data.

lows to handle self-occlusions of single parts of the hand and even to handle full rotations of the hand.

3.4 Finger Gesture Classification

Finger gestures are defined as specific finger poses, e.g., configurations of extended and not extended fingers. A well-known finger gesture is the OK sign where the thumb's and the index finger's tips touch each other and the remaining fingers are extended. The developed hand-finger pose estimation approach delivers the full hand configuration and is independent of the hand's size. Hence, it is predestinated for finger angle based gesture classification. Therefore, a support vector machine is trained with recorded hand-finger poses given by vectors containing the joint angles. For each gesture, only a few poses are recorded. The gesture names are based on their extended fingers from the thumb to the little finger, e.g., the OK sign is named MRL and the open hand leads to TIMRL. The fist and the so called vulcanian greeting are defined as additional gestures. The resulting gesture catalog contains 29 finger gestures.

The qualitative evaluation given in Section 4 presents skeleton model configurations inside the hand's 3D data for some of the defined gestures.

4 EVALUATION

The evaluation of the presented approach is split into five parts: pose estimation accuracy of the fingertips, correctness of the joint angle estimation, self-scaling ability, performance, and qualitative evaluation. For all tests, the Asus Xtion Pro RGB-D sensor is used.

To determine the *pose estimation accuracy*, a test subject performs four kinds of hand movements: abduction and adduction of the fingers (ABAD), flexion and extension of the fingers (FLEXEX), horizontal and vertical rotations of the hand of about 180° (ROT), and different movements like presenting a gesture (DIFF). In each frame, the visible fingertips are manually annotated and the tracking accuracy is determined as the root mean squared error of the fingertip features. The recorded evaluation sequences consist of 1385 frames.

The annotation of the data is based on the depth image and, consequently, the noise of the 3D data delivered by the camera is completely ignored. Therefore, an additional motion sequence (ROB) containing the real-world motion is recorded without camera noise. To achieve this, a self-made gypsum hand model on the basis of an impression of a test subject's hand is mounted on an Adept Viper industrial robot[1] and moved within a volume of 80 cm × 40 cm × 70 cm performing arbitrary translations as well as rotations. Furthermore, the hand's features are annotated manually: the fingertips, all finger joints and the center of the hand's root. To estimate the positions of the features for a given pose of the robot's effector, the hand model is measured using an NDI Polaris Spectra tracking system[2] and a previously calibrated transformation matrix between the robot's and tracking system's coordinate systems is used to estimate the transformation between the features and the effector. The robot's manually controlled movements with the gypsum hand are recorded with a Kinect at a distance of 170 cm in front of the robot while the effector's poses are logged and time synchronized. The features' mean values and a RANSAC-based SVD approach are used to determine the transformation between the robot's and the camera's coordinate systems. The evaluation sequence is about 2.2 min long

[1] www.adept.com

[2] www.ndigital.com

Table 2: The root mean squared errors of the finger tip nodes' distances from the corresponding ground truth data for all evaluation sequences.

	Root Mean Squared Error [mm]				
Motion	Little	Ring	Middle	Index	Thumb
AbAd	12.2	12.0	10.9	14.0	17.3
Diff	10.4	12.6	12.6	13.6	15.9
FlexEx	11.6	15.6	11.4	15.8	15.7
Rot	15.0	12.4	14.2	15.6	15.1
Rob	12.3	14.0	12.4	12.3	16.4
Mean	12.3	13.3	12.3	14.3	16.1

and 1832 frames are left after the synchronization due to a limited logging speed of the effector's poses to 13 Fps.

Table 2 illustrates the pose estimation accuracy of the fingertips for all sequences given as the root mean squared error (Rmse) of the distances between the ground truth and the determined poses. The mean tracking accuracy for the fingertips of the little finger and the middle finger is 12 mm, for the ring finger about 13 mm, for the index finger about 14 mm, and for the thumb about 16 mm. Further, the scaling factor is about 0.89 to 0.91 during all test sequences. The results show, that the pose estimation works correctly. There are several reasons for the resulting distances. They can be caused by the differences in the proportions of the model and the test subjects or the gypsum hand. The approach permits the scaling of the model, but the measured proportions of the fingers are fixed. The differences of the Rob sequence can be caused by the camera's noise. Finally, the manual annotation process can cause some differences. Because of the choice of the target joint positions as the mean value of all assigned points, the joint should not reach the margin of the hand data which was annotated beforehand.

Since just evaluating the tracking accuracy of the fingertips does not guarantee that the hand configuration is estimated correctly, additional evaluation is needed. There is no markerless system available which allows the determination of the joints' angles of a test subject's hand while it is recorded with a depth sensor. The evaluation of the *joint angle estimation's correctness* is thus based on a simulated hand model. Therefore, the hand of the virtual human being delivered by the Makehuman[3] framework was animated on the basis of hand and finger motions tracked beforehand. The determined model parameters are used as ground truth data and directly fed into the virtual hand. A virtual camera facing the hand's palm and the known camera model are used to emulate the Rgb-d sensor's 3D data. The motion sequence consists of sequential flexions and extensions of each finger from the little finger to the thumb followed by the presentation of the Imr, Iml, Irl, and Til gestures. Table 3 presents the results in the form of the Rmse of the recorded and tracked joints' angles for the full evaluation sequence consisting of 6080 frames. To obtain this sequence, the data simulation is repeated several times with a frame rate of 30 Fps. The mean Rmse is about 12.1° which indicates that the basic hand configuration is estimated correctly and should allow a gesture classification based on the joints' angles. The main reason for then differences between the angles is the animated virtual hand model, e.g., the flexion of the little finger as well as the most motions of the thumb result in abnormal distortions of the hand surface.

Table 3: The root mean squared errors of the joint angles for the tracking of the simulated hand model sequentially performing flexion and extension of each finger and presenting the gestures Imr, Iml, Irl and Til.

Finger	Root Mean Squared Error [°]			
	θ_{MCP1}	θ_{MCP2}	θ_{PIP}	θ_{DIP}
Little	17.5	18.3	10.6	5.5
Ring	9.2	13.3	6.8	9.9
Middle	9.3	14.2	6.1	8.4
Index	17.6	8.9	13.6	7.0
Thumb	24.8	16.6	13.4	10.0

To evaluate the *self-scaling ability*, a test subject presents his open hand and the scaling factor is determined manually as 0.9. Afterwards, the pose estimation approach is restarted with the different initial scaling factors 0.5, 0.8, 0.9, 1.0, and 1.5 corresponding to different steps of a too small and a too large scaling with respect to the manually determined value. In all cases, the approach ends up in scaling factors of 0.87 to 0.89 indicating a correct scaling. Facing the extreme cases of initial values of 0.5 and 1.5, the correct factors are reached after 1 to 3 frames.

[3] www.makehuman.org

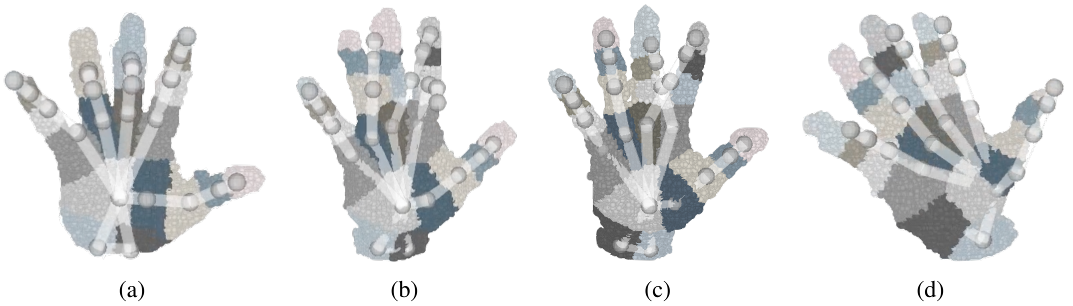

Figure 3: (a)-(b) Tracking failures caused by fast finger motions. (d) Model shift occurred during fast waving of the hand.

The *performance* is tested on two standard systems. The tracking algorithm is integrated in the ROS[4] framework and the delivered OpenNI driver is used for the RGB-D data acquisition. Vertical rotations of the open hand of a test subject at three different distances between the hand and the camera are qualitatively observed and the number of points belonging to the hand data are recorded. There are about 16,000 points inside the hand's point cloud at a distance of 0.5 m, 5,500 points at a distance of 1.0 m, and about 1,000 points at 2.0 m. The tracking is correct for all distances and the achieved performance represented by the frame rate of the hand poses is the same. On a Notebook with an Intel Core i7-2640M @ 2.80 GHz CPU, a frame rate of 24 FPS is achieved whereby the limitation is given by the data acquisition and not by the tracking algorithm. On a desktop computer with an Intel Core i7-3770 @ 3.40 GHz CPU, the real-time frame rate of 30 FPS is reached.

The tests show that, if necessary, a downsampling of the data is possible. This would reduce the computational complexity without affecting the quality of the pose estimation.

There is no annotated dataset publicly available which contains all the needed information, in this case, the additional data of the arm. Hence, a direct comparison with approaches like the ones presented in (Oikonomidis et al., 2010; Schröder et al., 2013; Sridhar et al., 2013; Qian et al., 2014) is not possible. However, the evaluation results show that the approach presented here is accurate in view of pose estimation and joint angle determination and much faster than the named approaches. Further, no large datasets recorded in advance are needed and the performance is obtained on standard hardware without using the GPU which predestinates this approach for embedded applications.

The *qualitative evaluation* is based on hand-finger motions in front of a static depth camera. Very fast finger movements can result in the loss of some model fingers exemplarily shown in Figure 3(a). Sometimes the fast extension of the middle and ring finger cannot be tracked due to a wrong point assignment based on large differences in the point clouds. Another problem with finger tracking is the displacement of neighbouring fingers, as illustrated in Figure 3(b). The tip of the middle finger is situated inside the real data of the tip of the index finger, lost beforehand. A rarely occurring tracking failure is shown in Figure 3(c), while the index and middle fingers are crossed. The reason for that are fast flexions and extensions of both fingers while performing small vertical rotations of the hand. Even the fast waving of the open hand can result in a little tracking shift, illustrated in Figure 3(d), which can be compensated after reducing the speed.

Some determined hand poses, while turning the open hand, are given by the first row of Figure 4. The approach allows to handle vertical rotations, whereas some incorrect tracking results occur while rotating the hand back (see Figure 4(d)). They are compensated when the initial pose, where the palm faces the camera, is reached. Figure 4(f)-(i) emphasize that partial self-occlusions, caused by configurations using sharp angles in between the palm of the hand and the camera, can be handled. Even poses while the back of the hand faces the camera or the hand is rotated in an arbitrary direction are estimated correctly and illustrated in Figure 4(j)-(n). Furthermore, the approach allows to adapt the model on gesture-specific hand configurations as shown in Figure 4(o)-(q). The model is also able to track gestures where some fingers are mostly parallel like the IML or the IMR gestures (see Figure 4(r) and Figure 4(s)). Qualitative tests show that the implemented *gesture classifier* is able to distinguish the 29 trained gestures. Even similar finger configurations like the open hand and the so called vulcanian greeting shown in Figure 4(e) and Figure 4(t) can be classified.

[4] www.ros.org

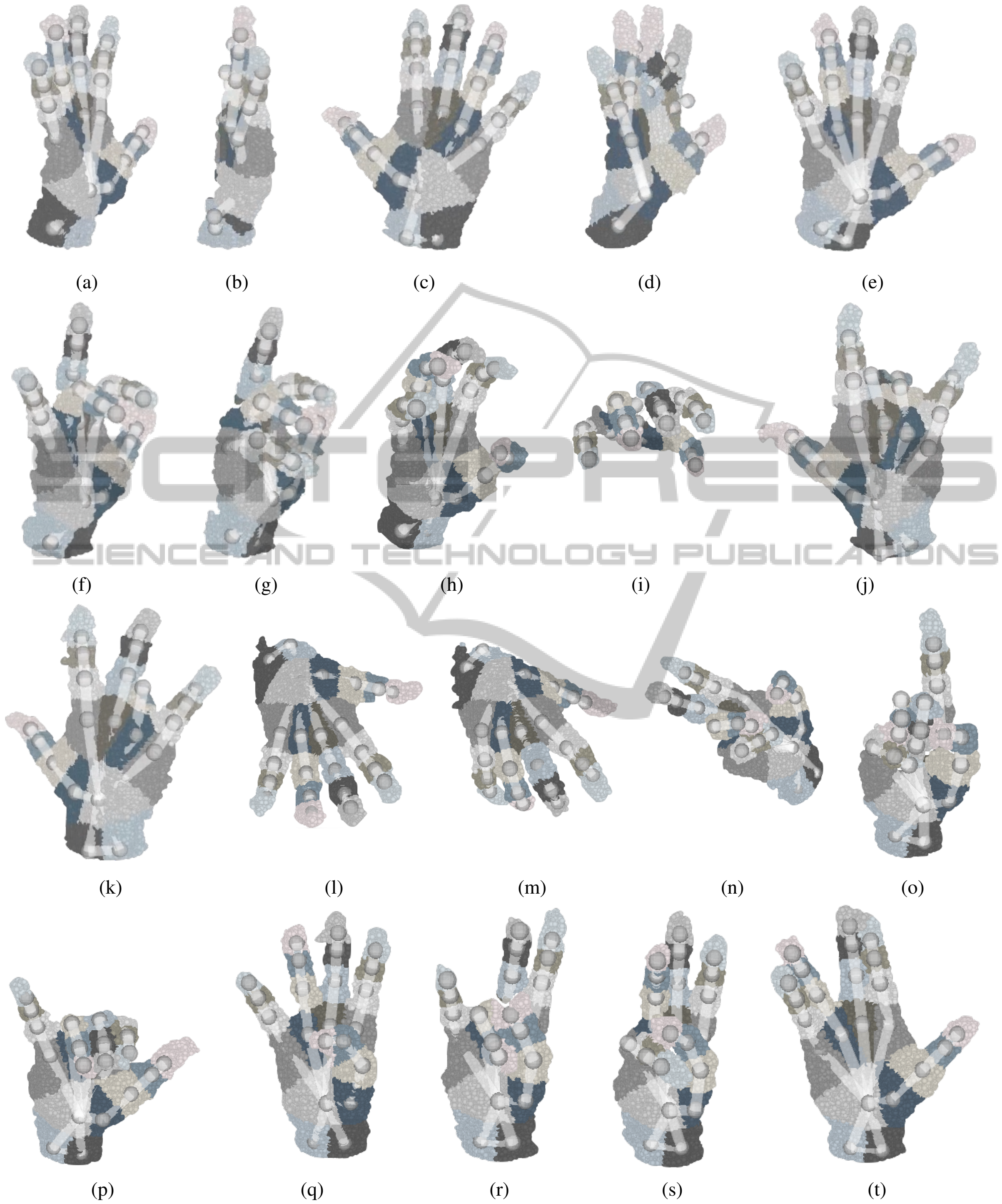

(a) (b) (c) (d) (e)

(f) (g) (h) (i) (j)

(k) (l) (m) (n) (o)

(p) (q) (r) (s) (t)

Figure 4: Determined hand skeleton model configurations with corresponding hand data. The first row shows some steps during the vertical rotation of the open hand of 180° and back. (f) - (i): The determined hand model in situations where there is a sharp angle between the camera and the hand's palm. (j) - (n): The pose can be tracked during arbitrary rotations and even when the back of the hand faces the camera. (o) - (t) show the model while presenting the gestures I, TL, IMRL, IML, IMR, and the so called vulcanian greeting. The priorly trained SVM is able to classify these gestures correctly.

5 CONCLUSION

In this paper, a real-time self-scaling kinematic hand skeleton model based approach for full hand-finger pose estimation while determining hand and finger joints' angles was presented. The model was iteratively adapted on the 3D data of the hand delivered by a depth camera using a least-squares optimization approach. Therefore, the data-model distance was simplified allowing the whole pose estimation process to be done in an optimization process without prior steps. Further, the model was equipped with a self-scaling ability to handle different hand sizes automatically.

A detailed evaluation of the approach was given including quantitative and qualitative results. It was shown that the approach allows to track the hand's skeleton under hard conditions such as turning the hand and presenting complex finger gestures. Furthermore, the tracking performance on standard hardware without using the GPU is up to 30 FPS, limited by the camera's speed. In addition, there are no training data or prior calculations required. Thus, the presented method is more efficient than most of the other known hand-finger tracking approaches.

Future work will focus on the remaining problems like handling very fast hand or finger movements and adaptable hand proportions. Some improvements on the support vector machine based gesture classifier and a quantitative evaluation are planned. In addition, an extension of the presented approach to estimating the arm pose or even the full body pose is intended. This would enable human robot interaction applications like controlling an industrial robot or a robotic hand and could be used for a simple teach-in procedure. Even simultaneous tracking of both hands and the body is planned.

REFERENCES

Aristidou, A. and Lasenby, J. (2010). Motion Capture with Constrained Inverse Kinematics for Real-Time Hand Tracking. In *International Symposium on Communications, Control and Signal Processing*, number March, pages 3–5.

Athitsos, V. and Sclaroff, S. (2003). Estimating 3D hand pose from a cluttered image. *2003 IEEE Computer Society Conference on Computer Vision and Pattern Recognition 2003 Proceedings*, 2:II–432–9.

Ballan, L., Taneja, A., Gall, J., Gool, L. V., and Pollefeys, M. (2012). Motion Capture of Hands in Action Using Discriminative Salient Points. In Fitzgibbon, A., Lazebnik, S., Perona, P., Sato, Y., and Schmid, C., editors, *Computer Vision – ECCV 2012*, volume 7577 of *Lecture Notes in Computer Science*, pages 640–653. Springer.

ElKoura, G. and Singh, K. (2003). Handrix: animating the human hand. *Eurographics symposium on Computer animation*.

Erol, A., Bebis, G., Nicolescu, M., Boyle, R. D., and Twombly, X. (2007). Vision-based hand pose estimation: A review. *Computer Vision and Image Understanding*, 108(1-2):52–73.

Gorce, M. D. L., Fleet, D. J., and Paragios, N. (2011). Model-Based 3D Hand Pose Estimation from Monocular Video. In *IEEE Transactions on Pattern Analysis and Machine Intelligence*, volume 33, pages 1793–1805. Laboratoire MAS, Ecole Centrale de Paris, Chatenay-Malabry, IEEE.

Han, J., Shao, L., Xu, D., and Shotton, J. (2013). Enhanced computer vision with Microsoft Kinect sensor: a review. *IEEE transactions on cybernetics*, 43(5):1318–34.

Horaud, R., Forbes, F., Yguel, M., Dewaele, G., and Zhang, J. (2011). Rigid and articulated point registration with expectation conditional maximization. *IEEE Transactions on Pattern Analysis and Machine Intelligence*, 33(3):587–602.

Keskin, C., , Kirac, F., Kara, Y. E., and Akarun, L. (2011). Real time hand pose estimation using depth sensors. In *Computer Vision Workshops (ICCV Workshops), 2011 IEEE International Conference on*, pages 1228–1234.

Keskin, C., , Kirac, F., Kara, Y. E., and Akarun, L. (2012). *Hand Pose Estimation and Hand Shape Classification Using Multi-layered Randomized Decision Forests*, volume 7577. Springer Berlin Heidelberg.

Lee, J. and Kunii, T. (1995). Model-based analysis of hand posture. *Computer Graphics and Applications, IEEE*, 15(5):77–86.

Liang, H., Yuan, J., and Thalmann, D. (2012). Hand Pose Estimation by Combining Fingertip Tracking and Articulated ICP. In *Proceedings of the 11th ACM SIGGRAPH International Conference on Virtual-Reality Continuum and Its Applications in Industry*, VRCAI '12, pages 87–90, New York, NY, USA. ACM.

Oikonomidis, I., Kyriazis, N., and Argyros, A. (2011). Efficient model-based 3D tracking of hand articulations using Kinect. *Procedings of the British Machine Vision Conference*, pages 101.1–101.11.

Oikonomidis, I., Kyriazis, N., and Argyros, A. A. (2010). Markerless and Efficient 26-DOF Hand Pose Recovery. *Hand The*, pages 744–757.

Qian, C., Sun, X., Wei, Y., Tang, X., and Sun, J. (2014). Realtime and Robust Hand Tracking from Depth. In *IEEComputer Vision and Pattern Recognition*.

Raheja, J. L., Chaudhary, A., and Singal, K. (2011). Tracking of Fingertips and Centers of Palm Using KINECT. *Third International Conference on Computational Intelligence Modelling Simulation*, pages 248–252.

Ren, Z., Meng, J., and Yuan, J. (2011). Depth Camera Based Hand Gesture Recognition and its Applications in Human-Computer-Interaction. *IEEE International*

Conference on Information Communication and Signal Processing, (1):3–7.

Ren, Z. and Yuan, J. (2011). Robust hand gesture recognition based on finger-earth mover's distance with a commodity depth camera. *Proceedings of the 19th ACM international*, pages 1–4.

Schröder, M., Elbrechter, C., Maycock, J., Haschke, R., Botsch, M., and Ritter, H. (2012). Real-Time Hand Tracking with a Color Glove for the Actuation of Anthropomorphic Robot Hands. In *Proceedings of IEEE-RAS International Conference on Humanoid Robots*, pages 262–269.

Schröder, M., Maycock, J., Ritter, H., and Botsch, M. (2013). Analysis of Hand Synergies for Inverse Kinematics Hand Tracking. In *IEEE International Conference on Robotics and Automation, Workshop of "Hand synergies - how to tame the complexity of grasping"*.

Shotton, J., Fitzgibbon, A., Cook, M., Sharp, T., Finocchio, M., Moore, R., Kipman, A., and Blake, A. (2011). Real-time human pose recognition in parts from single depth images. *IEEE Conference on Computer Vision and Pattern Recognition*, pages 1297–1304.

Sridhar, S., Oulasvirta, A., and Theobalt, C. (2013). Interactive Markerless Articulated Hand Motion Tracking Using RGB and Depth Data. *2013 IEEE International Conference on Computer Vision*, pages 2456–2463.

Wang, R., Paris, S., and Popović, J. (2011). 6D Hands: Markerless Hand-tracking for Computer Aided Design. In *Proceedings of the 24th Annual ACM Symposium on User Interface Software and Technology*, UIST '11, pages 549–558, New York, NY, USA. ACM.

Wang, R. Y. and Popović, J. (2009). Real-time hand-tracking with a color glove. *ACM Transactions on Graphics*, 28(3):1.

Wang, Y., Min, J., Zhang, J., Liu, Y., Xu, F., Dai, Q., and Chai, J. (2013). Video-based hand manipulation capture through composite motion control. *ACM Transactions on Graphics*, 32(4):1.

Zhao, W., Zhang, J., Min, J., and Chai, J. (2013). Robust realtime physics-based motion control for human grasping. *ACM Transactions on Graphics*, 32(6):1–12.